Supplementary Information for

Optically-controlled phonon-specific phase transitions from graphite to diamond

Yunzhe Jia,[1,2] Chenchen Song,[1,2] Daqiang Chen,[1,2] Qing Chen,[1,2] Cui Zhang,[1,3*] and Sheng Meng[1,2,3*]

[1]*Beijing National Laboratory for Condensed Matter Physics and Institute of Physics, Chinese Academy of Sciences, Beijing 100190, China*

[2]*School of Physical Sciences, University of Chinese Academy of Sciences, Beijing 100049, China*

[3]*Songshan Lake Materials Laboratory, Dongguan, Guangdong 523808, China*

[*]*E-mail: cuizhang@iphy.ac.cn; smeng@iphy.ac.cn*

Suppl. Note 1. Electron–phonon coupling calculation in real-time TDDFT molecular dynamics

The non-adiabatic molecular dynamic (NAMD) simulations performed here are within the framework of real-time time-dependent density functional theory (rt-TDDFT) and Ehrenfest dynamics. To solve the time-dependent Schrödinger equation,

$$\hat{H}_{mol}\Psi(\boldsymbol{r},\boldsymbol{R},t) = i\hbar\frac{\partial}{\partial t}\Psi(\boldsymbol{r},\boldsymbol{R},t),$$

the Hamiltonian is written as

$$\hat{H}_{mol}(\boldsymbol{r},\boldsymbol{R}) = -\sum_{\gamma}\frac{\hbar^2}{2M_\gamma}\nabla_\gamma^2 - \sum_{i}\frac{\hbar^2}{2}\nabla_i^2 + \sum_{i<j}\frac{1}{|\boldsymbol{r}_i-\boldsymbol{r}_j|} - \sum_{\gamma,i}\frac{Z_\gamma}{|\boldsymbol{R}_\gamma-\boldsymbol{r}_i|} + \sum_{\gamma<\zeta}\frac{Z_\gamma Z_\zeta}{|\boldsymbol{R}_\gamma-\boldsymbol{R}_\zeta|}.$$

Within the theoretical framework of Ehrenfest dynamics that we have adopted, the total wave function is expressed in the following form,

$$\Psi(\boldsymbol{r},\boldsymbol{R},t) = \Phi(\boldsymbol{r},t)\Omega(\boldsymbol{R},t)exp\left[\frac{i}{\hbar}\int_{t_0}^{t}dt' E_{el}(t')\right],$$

$$E_{el}(t) = \iint d\boldsymbol{r}d\boldsymbol{R}\Phi^*(\boldsymbol{r},t)\Omega^*(\boldsymbol{R},t)\hat{\mathcal{H}}_{el}(\boldsymbol{r},\boldsymbol{R})\Phi(\boldsymbol{r},t)\Omega(\boldsymbol{R},t).$$

Based on this, the respective evolution equations for the electronic and ionic subsystems can be derived as

$$i\hbar\frac{\partial\Phi(\boldsymbol{r},t)}{\partial t} = -\frac{\hbar^2}{2}\sum_i\nabla_i^2\Phi(\boldsymbol{r},t) + \left[\int d\boldsymbol{R}\,\Omega^*(\boldsymbol{R},t)\hat{V}(\boldsymbol{r},\boldsymbol{R})\Omega(\boldsymbol{R},t)\right]\Phi(\boldsymbol{r},t),$$

$$i\hbar\frac{\partial\Omega(\boldsymbol{R},t)}{\partial t} = -\frac{\hbar^2}{2}\sum_\gamma M_\gamma^{-1}\nabla_\gamma^2\Omega(\boldsymbol{R},t) + \left[\int d\boldsymbol{r}\,\Phi^*(\boldsymbol{r},t)\hat{\mathcal{H}}_{el}(\boldsymbol{r},\boldsymbol{R})\Phi(\boldsymbol{r},t)\right]\Omega(\boldsymbol{R},t).$$

Indeed, both the electronic and ionic subsystems evolve within mean fields determined by each other's real-time states. Consequently, the electron–phonon coupling also evolves in real time. This treatment represents a notable advantage of the real-time time-dependent density functional theory (rt-TDDFT) dynamics approach we have adopted, as it constitutes a first-principles methodology.

2. Distribution of photoexcited charge carriers

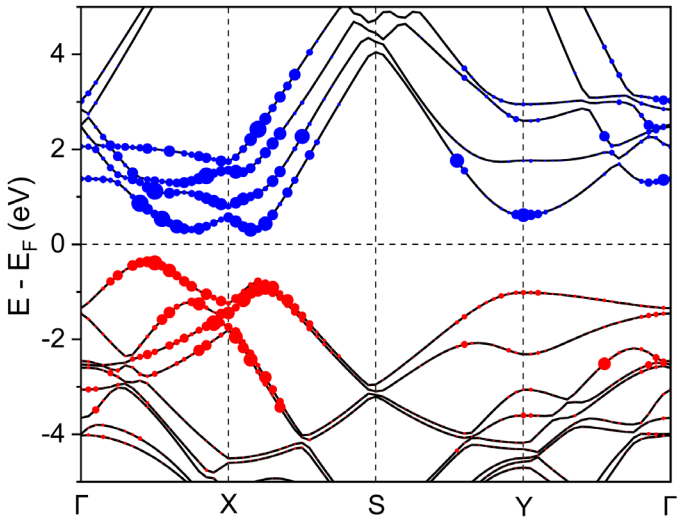

Suppl. Fig. 1. Distribution of photoexcited electrons and holes on the band structure during graphite-to-diamond phase transition, extracted from the rt-TDDFT MD simulation at the end of laser pulse t= 96 fs. The sizes of blue and red dots are proportional to the square of the population of excited electrons and holes generated by the laser pulse with respect to the ground state. (The largest dot represents $\Delta q \approx 1.66\ e$.)

3. Ionic temperature evolution during structural relaxation process

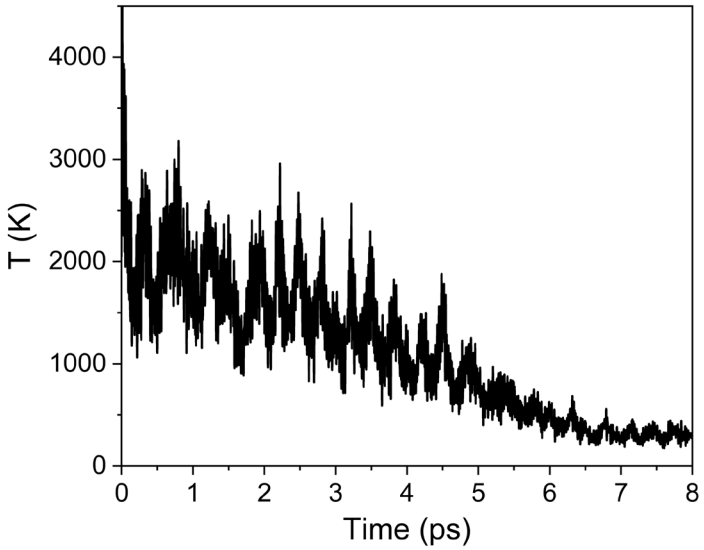

Suppl. Fig. 2. Time evolution of ionic temperature during the structural relaxation process. Time zero here corresponds to 0.4 ps in Fig. 2

4. Time evolution of the number of interlayer bonds

The number of interlayer C-C bonds N_{IB} is calculated from the trajectory shown in Fig. 2b. Only interlayer bonds connecting atoms between the two graphene layers within the same supercell are counted, therefore, N_{IB}=4 per layer means all atoms in the 16-atom supercell are involved in interlayer bonding.

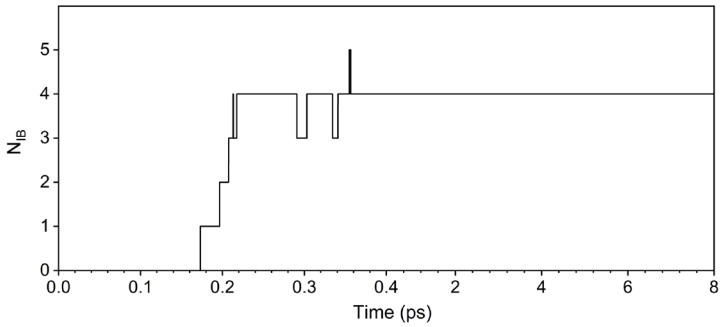

Suppl. Fig. 3. Time evolution of the number of interlayer C-C bonds (N_{IB}) formed during the phase transition process from graphite to cubic diamond.

5. Time-dependent electron localization function

Time-dependent electron localization function is calculated using the expression[1]

$$TDELF(\boldsymbol{r}) = \frac{1}{1+\left(\frac{D(\boldsymbol{r})}{D_0(\boldsymbol{r})}\right)^2}$$

in which

$$D(\boldsymbol{r}) = \tau(\boldsymbol{r}) - \frac{1}{4}\frac{|\nabla\rho(\boldsymbol{r})|^2}{\rho(\boldsymbol{r})}, \qquad D_0(\boldsymbol{r}) = \frac{3}{5}(6\pi^2)^{2/3}\rho(\boldsymbol{r})^{2/3}$$

In the above expressions, $\rho(\boldsymbol{r})$ represents the total charge density. $\tau(\boldsymbol{r})$ and $D_0(\boldsymbol{r})$ are kinetic energy densities of the system and uniform electron gas, respectively. In our work, each Time-dependent Kohn-Sham (TDKS) orbital is spin-degenerate, thus

$$\tau(\boldsymbol{r}) = \frac{1}{2}\sum_{i=1}^{n_{occ}}\left|\nabla\psi_i^{TDKS}(\boldsymbol{r})\right|^2, \qquad \rho(\boldsymbol{r}) = \sum_{i=1}^{n_{occ}}\left|\psi_i^{TDKS}(\boldsymbol{r})\right|^2$$

while each orbital obeying the condition of normalization

$$\iiint_{cell}\left|\psi_i^{TDKS}(\boldsymbol{r})\right|^2 d\boldsymbol{r} = 2$$

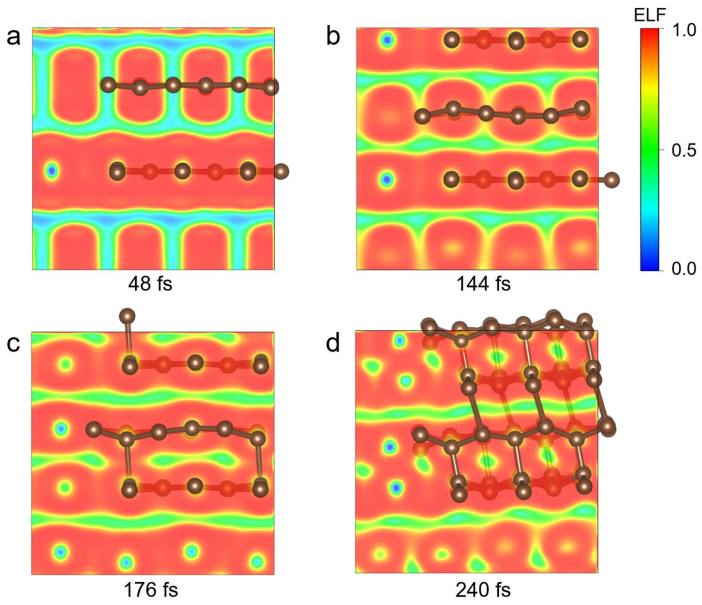

Suppl. Fig. 4. Time-dependent electron localization function (TDELF) analysis at (a) 48 fs, (b) 144fs, (c) 176 fs and (d) 240 fs during the phase transition process.

6. Differential charge density cross section

The charge densities of the excited states of the system are obtained from TDAP trajectory, while those of ground states are derived from self-consistency calculations using SIESTA software. The differential charge densities are calculated by subtracting the ground-state charge density from the excited state ones. Cross sections are cut along (100) plane. Such differential charge densities reflect the orbital shape near the Fermi surface. After 160 fs, interlayer bonds form and the orbital shapes change from sp^2-type to sp^3-type.

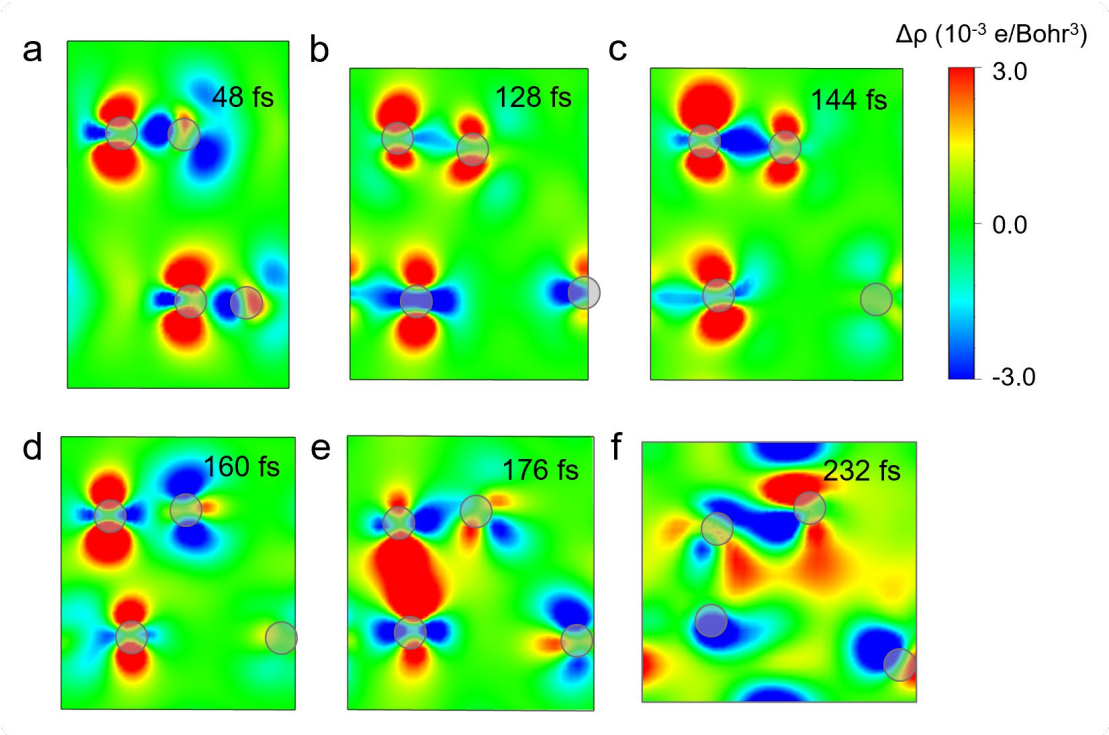

Suppl. Fig. 5. Differential charge density cross section of the TDAP trajectory in Fig. 2 at several moments. The gray circles mark the approximate positions of the atoms.

7. Annealing process initiating from the state at 280 fs in the non-adiabatic simulation

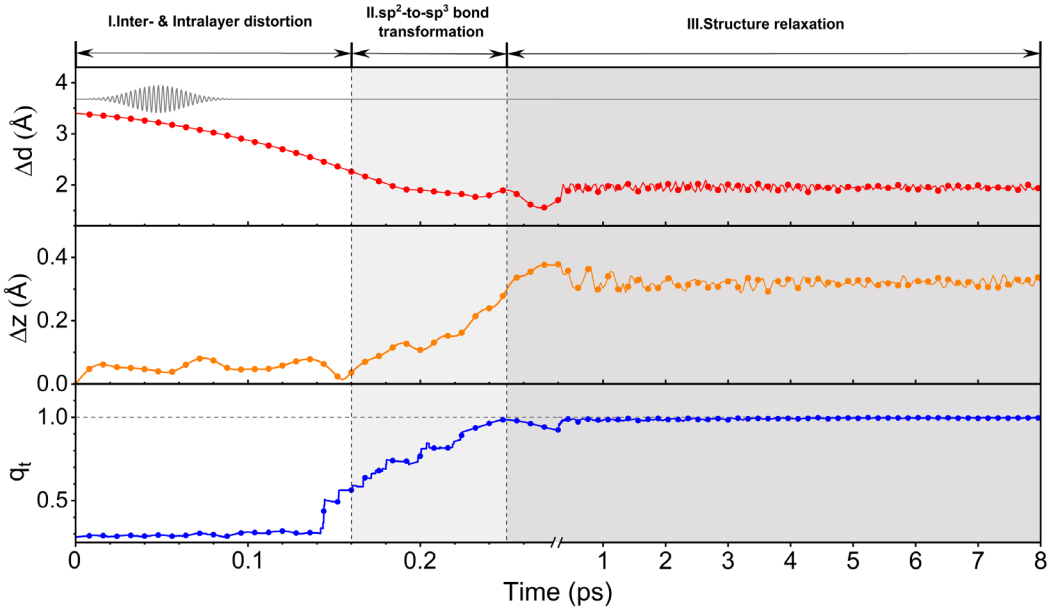

Suppl. Fig. 6. Time evolution of the interlayer spacing Δd, intralayer buckling height Δz and tetrahedral order parameter q_t of graphite. The annealing process starts with the state obtained at 280 fs in the non-adiabatic simulation and continues up to 8.0 ps.

8. Phase transition process from *AA* stacked graphite

Laser-induced phase transition from *AA* stacked graphite also contains three main stages. Before 200 fs, mean distance between adjacent layers Δd decrease from 3.4 Å to ~2.0 Å. Meanwhile, interlayer sliding and slightly intralayer buckling also appear. From 200 fs to 250 fs, Δz increase rapidly, accompanied with the formation of interlayer bonds. After 250 fs, Δd, Δz and N_{IB} all maintain at a relatively stable state, which indicates that the system has entered relaxation process.

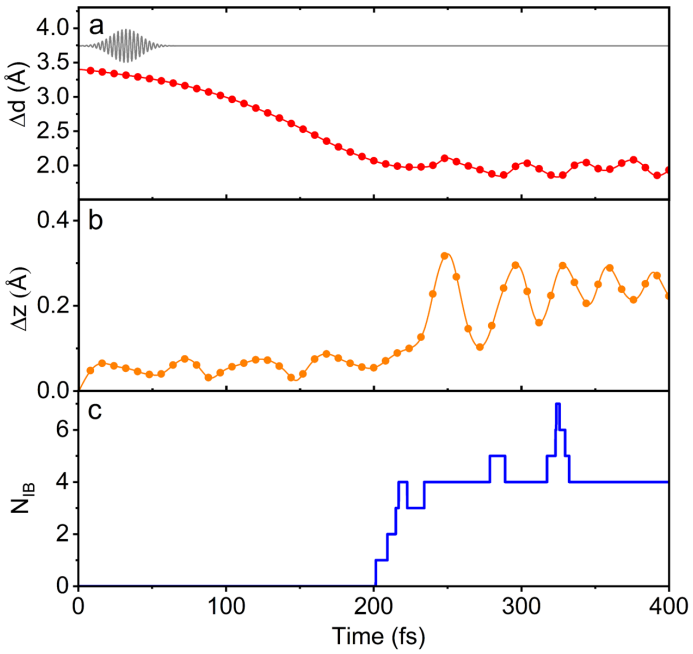

Suppl. Fig. 7. Time evolution of the electric field(E) of laser pulse, mean distance Δd(**a**), the mean intralayer buckling height Δz(**b**) and number of interlayer C-C bonds N_{IB}(**c**) of rt-TDDFT trajectory from AA stacked graphite are plotted in grey, red orange and blue lines, respectively. The field strengths of Gaussian-shaped laser pulses act on *AA* stacked graphite are E_0 = 0.514 V/Å, and the fluence is 80.3 mJ/cm^2. Accordingly, full widths at half maximum (FWHM) are 20 fs, while the laser field reaches the maximum strength E_0 at 32 fs.

9. Time evolution of electron excitation ratio

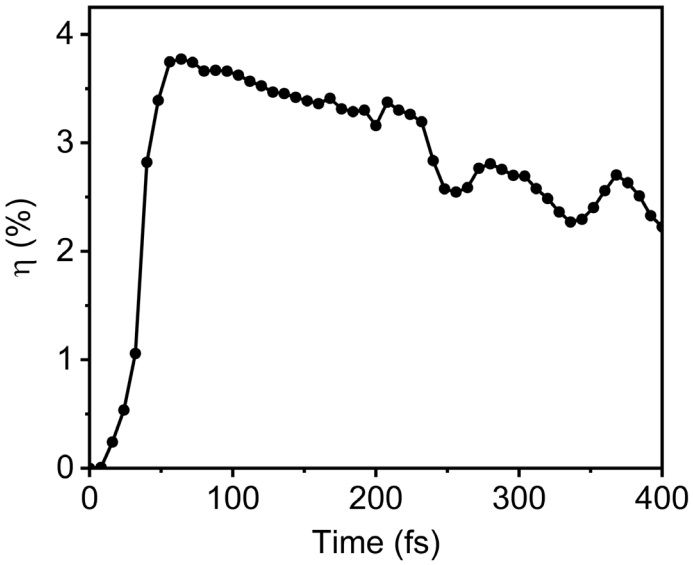

Suppl. Fig. 8. Time evolution of percentage of excited electrons η for trajectory in Fig. 2.

10. Phonon-phonon coupling between B_{3g}^{1} and B_{3g}^{2} modes

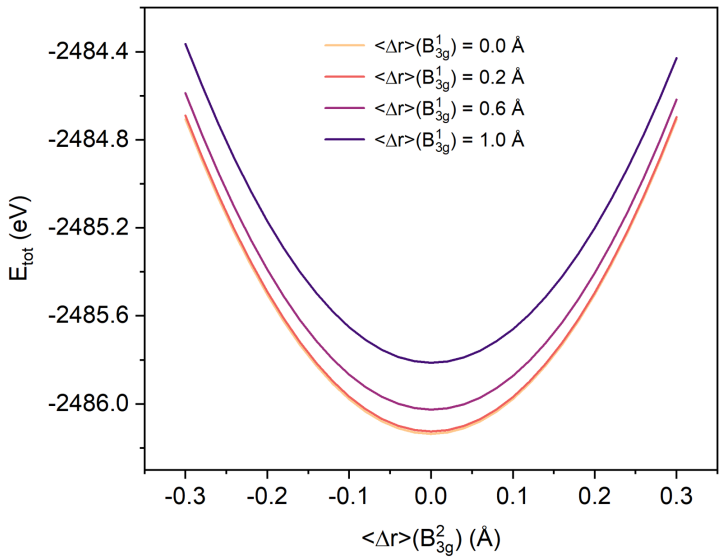

Suppl. Fig. 9. Potential energy surfaces of B_{3g}^{2} mode, corresponding to different displacements $\langle \Delta r \rangle$ of B_{3g}^{1} mode. $\langle \Delta r \rangle$ denotes the average displacement of all atoms along a specific phonon

11. Time evolution of the average atomic displacement of excited phonons

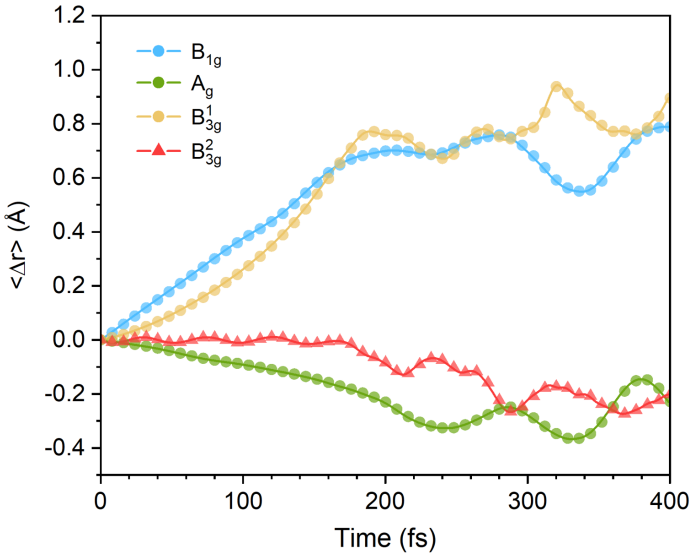

Suppl. Fig. 10. Time evolution of the four primarily excited phonon motions at Γ point during the graphite phase transition to cubic diamond. $\langle \Delta r \rangle$ represents the average atomic displacement of each phonon mode along the polarization vector direction.

12. Phonon dispersion spectrum and vibrational modes of graphite

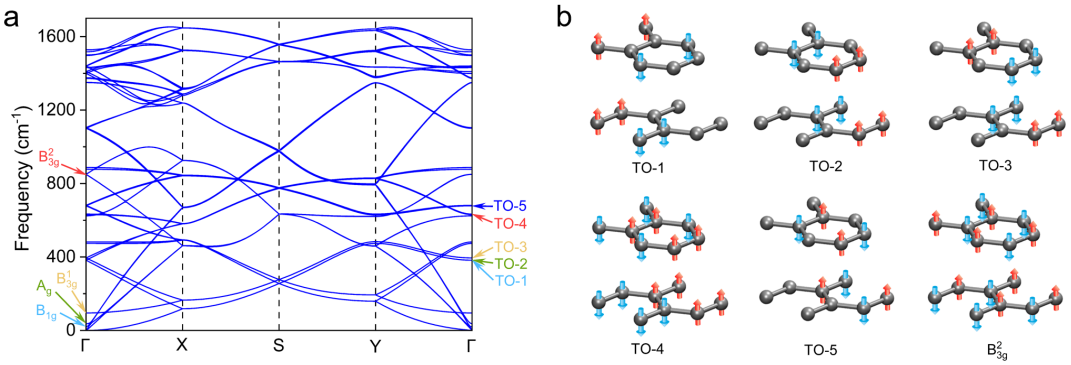

Suppl. Fig. 11. **a** Phonon dispersion spectrum of supercell of *AB* stacked graphite. Several main phonons mentioned in Fig. 4 are marked beside the corresponding frequencies. **b** Vibrational modes of six representative phonons participated in the competition to determine the final product, which are mentioned in Fig. 4c. Different colored arrows indicate different directions of atomic motions.

13. Time evolution of the bond parameter Q during phase transitions

The Q = 0 and Q = 1 shown in Fig. S13b refer to the bond parameters for a specific C–C bond, staggered vs. eclipsed. For HD structure, the ratio of staggered to eclipsed C–C bonds is 1:3, thus an ideal average value $\langle \boldsymbol{Q} \rangle$ for HD phase should be 0.75.

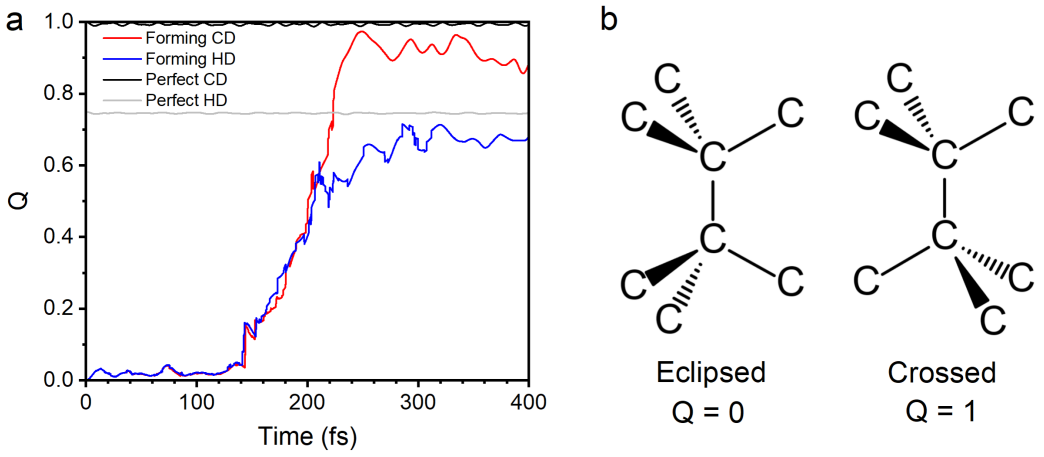

Suppl. Fig. 12. a Time evolution of bond parameter Q corresponding to trajectories forming CD (red line) and HD (blue line), compared with those corresponding to perfect CD (black line, $\langle Q \rangle \approx 1$) and HD (grey line, $\langle Q \rangle \approx 0.75$) under 300 K. **b** Schematic figure of Q values corresponding to a single C–C bond in either the perfectly eclipsed or crossed conformation.

14. Crucial role of eletron excitation amount in graphite phase transitions

The color of each data point in the diagram corresponds to the average of the maximum percentage of excited electrons for several trajectories under each optical parameter. As shown in Fig. 5b and Fig. S13a, although the laser fluence required to induce graphite-to-diamond phase transformation gradually decreases with increasing wavelength, it tends to saturate in range of 900–1000 nm, indicating the existence of a minimum intensity threshold. This trend is established under the premise of achieving a specific excitation level. In regions with low photon energy (*e.g.*, the microwave field), it is difficult to reach the approximately 3–4% electron excitation threshold required to drive strong phonon excitation for the *sp²-to-sp³* structural phase transition.

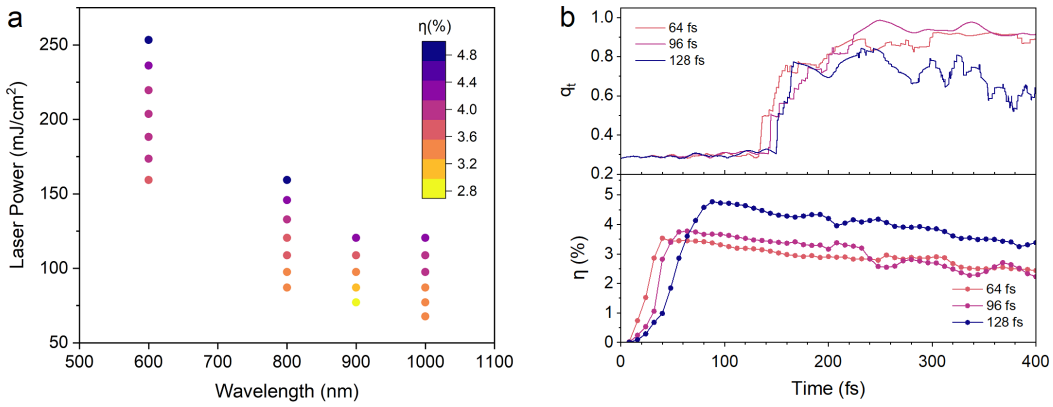

Suppl. Fig. 13. a Maximum percentage η of excited electrons in graphite under different laser parameters. **b** Time evolution of the tetrahedral order parameter q_t and percentage of excited electrons η for different pulse duration.

15. Size effects on the photoinduced graphite phase transition

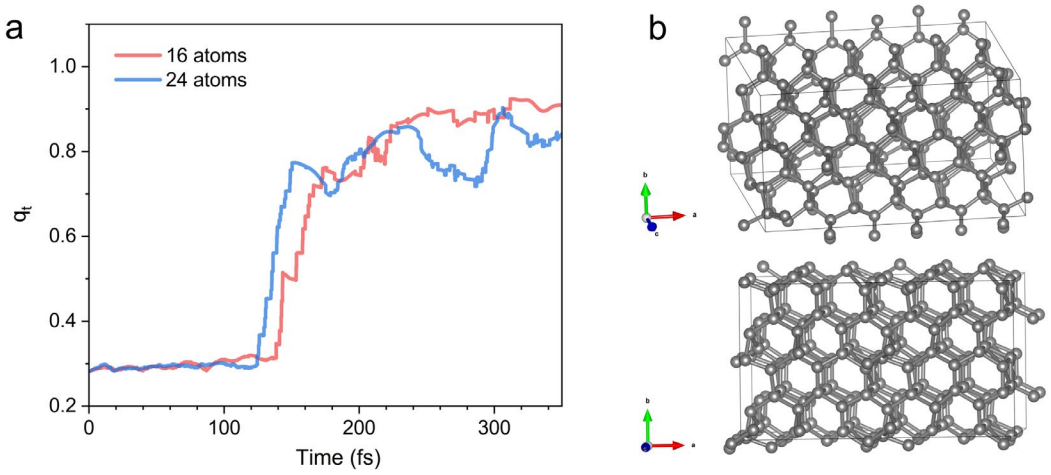

Suppl. Fig. 14. a Time evolution of the tetrahedral order parameter q_t for two trajectories with different cell size and both forming HD phase. **b** Structures of 16-atom (top) and 24-atom (bottom) trajectories at ~300 fs. The top and bottom figures have undergone 3×2×2 and 2×2×2 supercell expansions, respectively, to ensure the consistent on total number of atoms.

16. Influence of light polarization direction

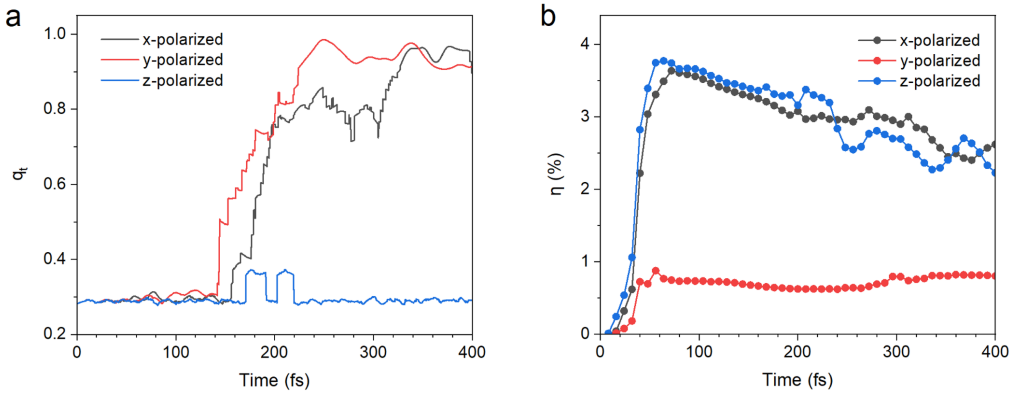

Suppl. Fig. 15. a Time evolution of the tetrahedral order parameter q_t for different pulse durations (64 fs, 96 fs and 120 fs). **b** Time evolution of the percentage of excited electrons η

Supplementary references

1. Becke, A. D. & Edgecombe, K. E. A simple measure of electron localization in atomic and molecular systems. *J. Chem. Phys.* **92**, 5397-5403 (1990).